CHEMISTRY
A European Journal

A Journal of
ChemPubSoc Europe

Accepted Article

Title: Anticancer Ir(III)-Aspirin Conjugates for Enhanced Metabolic Immuno-Modulation and Mitochondrial Lifetime Imaging

Authors: Xiao-Wen Wu, Yue Zheng, Fang-Xin Wang, Jian-Jun Cao, Hang Zhang, Dong-Yang Zhang, Cai-Ping Tan, Liang-Nian Ji, and Zong-Wan Mao

To be cited as: *Chem. Eur. J.* 10.1002/chem.201900851

Link to VoR: http://dx.doi.org/10.1002/chem.201900851

Supported by
ACES

WILEY-VCH

10.1002/chem.201900851

WILEY-VCH

Anticancer Ir(III)-Aspirin Conjugates for Enhanced Metabolic Immuno-Modulation and Mitochondrial Lifetime Imaging

Xiao-Wen Wu,[†][a] Yue Zheng,[†][a] Fang-Xin Wang,[a] Jian-Jun Cao,[a] Hang Zhang,[a] Dong-Yang Zhang,[a] Cai-Ping Tan,*[a] Liang-Nian Ji[a] and Zong-Wan Mao*[a]

Abstract: The chemo-anti-inflammatory strategy is gaining more and more attention in the treatment of cancer. Herein, two cyclometalated Ir(III) complexes **Ir2** and **Ir3** formed by conjugation of **Ir1** with two antiphlogistics (aspirin and salicylic acid) have been designed. **Ir2** and **Ir3** exhibit higher antitumor and anti-inflammatory potencies than a mixture of **Ir1** and aspirin/salicylic acid. We show that they can be hydrolyzed, accumulate in mitochondria, and induce mitochondrial dysfunction. Due to their intense long-lived phosphorescence, **Ir2** and **Ir3** can track mitochondrial morphological changes. Phosphorescence lifetime imaging shows that **Ir2** and **Ir3** can aggregate during mitochondrial dysfunction. As expected, **Ir2** and **Ir3** exhibit immunomodulatory properties by regulating the activity of the immune factors. Both **Ir2** and **Ir3** can induce caspase-dependent apoptosis and caspase-independent paraptosis and inhibit several events related to metastasis. Moreover, **Ir2** and **Ir3** show potent tumor growth inhibition *in vivo*. Our study demonstrates that the combination of mitochondrial targeting and immunomodulatory activities is feasible to develop multifunctional metal-based anticancer agents.

Introduction

Though platinum drugs like cisplatin have achieved great success, their development is hindered by drug resistance and severe side effects.[1] Other non-platinum complexes may be able to overcome cisplatin resistance if they have different mechanisms of actions. Among them, organometallic metal complexes show promise for overcoming the platinum resistance, e.g., Ru(II)/Ir(III) arene complexes and cyclometalated Ir(III) complexes.[2-4] Notably, iridium complexes are getting wide attention for biological applications, especially organometallic iridium complexes.[3] Cyclometalated Ir(III) complexes demonstrate interesting antitumor properties, e.g., inhibiting protein-protein interactions and targeting subcellular organelles.[4] In immunotherapy for cancer, iridium complexes have also shown potential applications in molecular imaging,[5] protein inhibition[6-8] and inflammatory modulation.[9] On the other hand, iridium complexes are promising bioimaging materials because of their high emission quantum yields and good photostability.[10-15] Due to their triplet emissive states, phosphorescent iridium complexes have large Stoke shifts that can minimize the self-quenching effects.[16] They also have long-lived phosphorescence that is much longer than the lifetimes of cellular background fluorescence (less than 10 ns) and organic dyes commonly used in cell imaging.[11-12, 14] Therefore, iridium complexes can be applied in time-gate imaging to avoid the interference from short-lived scattering and autofluorescence.[12, 14] The long lifetime of iridium complexes can also applied in phosphorescence lifetime imaging (PLIM) to quantitatively detect the analytes more accurately.[12, 14]

Inflammatory responses play important roles at different stages of tumor development.[17] It has been reported that 18% of human malignancies are linked to infectious agents.[18] Aspirin (**As**), a salicylic acid (**SA**)-based medicine, is widely used as an analgesic, antipyretic and anti-inflammatory medicine. Many clinical studies have shown that long-term daily **As** use has an antitumor effect.[19-21] Some successful chemotherapeutics can induce a type of immunogenic cancer cell death,[22] and in turn anticancer immune responses may make effect to control cancer.[23] A chemo-anti-inflammatory molecule that can release active anticancer drugs and anti-inflammatory agents concurrently upon cellular activation is a potent approach to treat stubborn cancers. For example, the platinum(IV) prodrug Platin-A designed by Shanta[24] and Liu[25-26] exhibits both anticancer and anti-inflammatory properties.

Mitochondria show important functions in physiological and pathological conditions.[27] Cancer cells display different degrees of transformations in mitochondrial functions,[28-29] which provides opportunities to target mitochondria for the treatment of cancer.[27, 30] Moreover, accumulating evidence shows that mitochondria also play important roles in the establishment and functions of immune cell phenotypes.[31-34] As previous researches have indicated that mitochondrial energetics and metabolism are interconnected with immuno-response, we purpose that the combination of mitochondria-targeting with immunomodulatory properties may present an effective strategy to obtain anticancer agents with novel mechanisms of action.

In this work, we designed two Ir(III)-antiphlogistics hybrid complexes with both mitochondria-targeted capabilities and immunomodulary activities. $[Ir(ppy)_2(L2)](PF_6)$ (**Ir2**; ppy: 2-phenylpyridine; L2: [2,2'-bipyridine]-4,4'-diylbis(methylene) bis(2-hydroxybenzoate)) and $[Ir(ppy)_2(L3)](PF_6)$ (**Ir3**; L3: [2,2'-bipyridine]-4,4'-diylbis(methylene) bis(2-acetoxybenzoate)) were obtained by conjugating **SA** or **As** with the cyclometalated Ir(III) complex $[Ir(ppy)_2(L1)](PF_6)$ (**Ir1**; L1: 4,4'-bis(hydroxymethyl)-2,2'-bipyridine) by ester bonds (Figure 1A). Due to their positive charge and lipophilicity, **Ir1**–**Ir3** were anticipated to accumulate in mitochondria. The hydrolysis of ester bonds, the cytotoxicity

[a] X. Wu, Y. Zheng, F. Wang, J. Cao, H. Zhang, Dr. D. Zhang, Dr. C. Tan, Prof. L. Ji, Prof. Z. Mao
MOE Key Laboratory of Bioinorganic and Synthetic Chemistry
School of Chemistry, Sun Yat-Sen University
Guangzhou 510275 (P.R. China)
Email: cesmzw@mail.sysu.edu.cn; tancaip@mail.sysu.edu.cn
† These authors contributed equally to this work.

Supporting information for this article is given via a link at the end of the document.((Please delete this text if not appropriate))

and cellular uptake properties of **Ir2** and **Ir3** were investigated. Their anti-inflammatory properties in inhibition of pro-inflammatory cytokines were evaluated. Their anticancer mechanisms, e.g., cell death modes, the impact on mitochondrial functions and several events related to metastasis including migration, colony-formation and angiogenesis, were illustrated. Finally, the *in vivo* anticancer efficacy was evaluated in a human tumor xenograft model. The applications of **Ir2** and **Ir3** in tracking of mitochondrial morphology and lifetime imaging were also demonstrated. In all, our study shows that the combination of mitochondrial targeting and immunomodulary activities is a feasible strategy to develop novel metal-based anticancer agents.

Results and Discussion

Synthesis, Characterization and Hydrolysis of the Ester Bonds

The structures of **Ir1**–**Ir3** are shown in Figure 1A. Ligands **L2** and **L3** were prepared by condensation of 4,4'-bis(bromomethyl)-2,2'-bipyridine with **SA**/**As** under weak basic conditions in dry N,N-dimethyl formamide (DMF). **Ir1** was prepared by the literature method.[35] **Ir2** and **Ir3** were synthesized similarly by reacting the Ir(III) precursors with the corresponding ligands in CH_2Cl_2/CH_3OH (1:1, v/v). The ligands (**L2** and **L3**) and the complexes (**Ir2** and **Ir3**) were characterized by ESI-MS (Figure S1–S4), ^{1}H NMR (Figure S5–S8), ^{13}C NMR (Figure S9–S12) and elemental analysis.

The photophysical properties of **Ir2** and **Ir3** in CH_3CN, CH_2Cl_2 and phosphate buffered saline (PBS) were tested (Figure S13, S14 and Table S1). The high-energy bands (< 350 nm) are the spin-allowed ligand-centered (^{1}LC) π-π* transitions for the cyclometalated (C–N) and the ancillary (N–N) ligands. The relatively low-energy bands can be assigned to the mixed singlet and triplet metal-to-ligand charge-transfer (^{1}MLCT and ^{3}MLCT) and ligand-to-ligand charge-transfer (LLCT) transitions. **Ir2** and **Ir3** exhibit orange red phosphorescent emissions upon excitation at 405 nm. The phosphorescence lifetimes of **Ir2** and **Ir3** in CH_3CN, CH_2Cl_2 and PBS fall between 64 and 631 ns.

The responses of **Ir2**–**Ir3** towards esterase were monitored by time-resolved emission spectra and ESI-MS. Time-dependent emission studies show that the emission spectra of **Ir2** and **Ir3** display a decrease in the intensities upon treatment with porcine liver esterase (PLE, Figure 1B and 1C). Also, the mass spectra show that **Ir2** and **Ir3** are completely hydrolyzed within 4 h upon treatment with PLE (Figure S15 and S16).

In Vitro Cytotoxicity

The cytotoxicity of **Ir1**–**Ir3**, **As**, **SA**, a 2-fold molar ratio of **As** or **SA** mixed with **Ir1**, and cisplatin was determined against prostate carcinoma (PC3), colon carcinoma (CT26) and human colon adenocarcinoma (HT29) cells by the

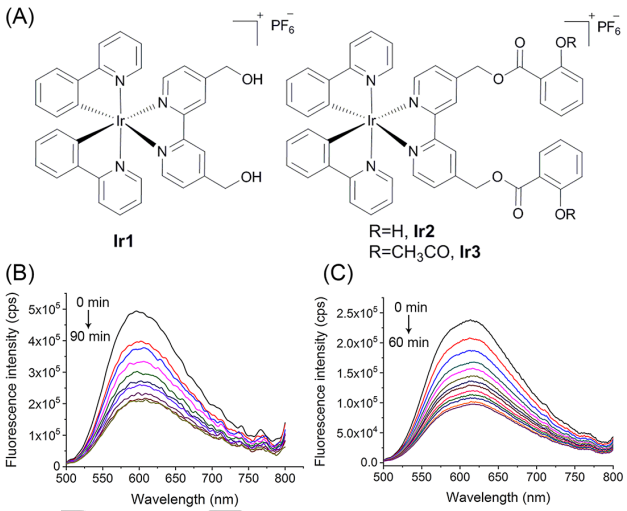

Figure 1. (A) The chemical structures of complexes **Ir1**–**Ir3**. Time-dependent emission spectra of **Ir2** (B) and **Ir3** (C) in the presence of PLE measured in PBS.

3-(4,5-dimethylthiazol-2-yl)-2,5-diphenyltetrazolium bromide (MTT) assay after 48 h treatment (Table 1). These cell lines were chosen because they were reported to be sensitive to **As** treatment.[24, 36] The IC_{50} values of **Ir2** and **Ir3** fall between 2.0 and 4.5 μM. Both **Ir2** and **Ir3** show higher toxicity than cisplatin (up to 10-fold). With IC_{50} values higher than 200 μM, both **As** and **SA** show negligible cytotoxicity. The result is in accordance with the literature report indicating that **As** needs millimolar doses to elicit cytotoxicity.[37] **Ir1** shows moderate cytotoxicity with IC_{50} values in the range between 91.2 and 100 μM. In contrast, the mixtures of 2-fold molar ratio of **As** or **SA** with **Ir1** do not show much improved cytotoxicity as compared with **Ir1** alone. These results indicate that the ligation of **As**/**SA** to Ir(III) complexes can achieve a superior synergistic effect on killing cancer cells.

Immunomodulatory Properties

Pro-inflammatory cytokines including interleukin (IL)-6 and tumor necrosis factor alpha (TNF-*α*), are of great importance for malignant proliferation, cancer progression, metastasis and evasion of immune surveillance.[24, 38] Meanwhile, they are also considered to be key growth-promoting and antiapoptotic factors that can protect cancerous cells from apoptosis.[39] The effects of **Ir1**−**Ir3**, a combination of **Ir1** with **As**/**SA**, and **As**/**SA** alone on IL-6 and TNF-*α* levels in lipopolysaccharide (LPS)-activated RAW 264.7 macrophage-like cells mimicking the inflammatory environment in cancer were evaluated by ELISA (Enzyme Linked Immunosorbent Assay). A concentration-dependent inhibition on IL-6 and TNF-*α* is observed for both preventative (Figure 2A and 2B) and therapeutic anti-inflammatory treatment (Figure 2C and 2D). The level of IL-6 is significantly

Table 1. IC_{50} values of tested compounds to different cells[a]

Compound	IC50 (μM)		
	PC3	CT26	HT29
Ir1	> 100	> 100	91.2 ± 2.1
Ir2	2.0 ± 0.4	2.2 ± 0.3	2.7 ± 0.3
Ir3	4.5 ± 0.5	4.4 ± 0.7	2.8 ± 0.3
Ir1+2 SA	54.9 ± 2.6	> 100	56.2 ± 3.1
Ir1+2 As	63.1 ± 2.3	> 100	85.1±6.6
SA	> 200	> 200	> 200
As	> 200	> 200	> 200
cisplatin	25.1 ± 2.2	22.4 ± 2.6	70.8 ± 4.5

[a] Cell viability was evaluated after 48 h incubation.

reduced by 2.1–19.4 fold in LPS-activated macrophages treated with **Ir2** or **Ir3**. Similar results are also observed for TNF-*α* production, which is decreased by 2.1–21.1 fold in cells treated with **Ir2** and **Ir3**. However, **Ir1**, **As**, **SA** and the mixtures of **Ir1** and **As**/**SA** show moderate effect on the levels of these cytokines under the same conditions.

Cyclooxygenase (COX), a vital enzyme in prostaglandin generation, is considered to be main target of **As**.[40] There are two isoforms COX in which constitutive overexpression of COX-2 is associated with resistance to apoptosis, which is the hallmark of cancer cells.[41] *In vitro* COX-2 inhibitory screening shows that **Ir3** displays potent inhibition on COX-2, close to that observed for **As** (Figure 2E). A much lower inhibitory activity is observed for **Ir2** and **SA** which is reasonable because **As** is more effective than **SA** as an inhibitor of COX.[42] Since many cancerous cells including PC3 cells over-express COX-2,[43] we next investigated whether **Ir3** could also influence the COX-2 expression in PC3 cells. An obviously down-regulated expression level of COX-2 is observed in cells treated with **Ir3** (Figure 2F), which is similar to that observed for **As**. The result indicates that COX-2 inhibition may contribute to the immunomodulatory properties of **Ir3**.

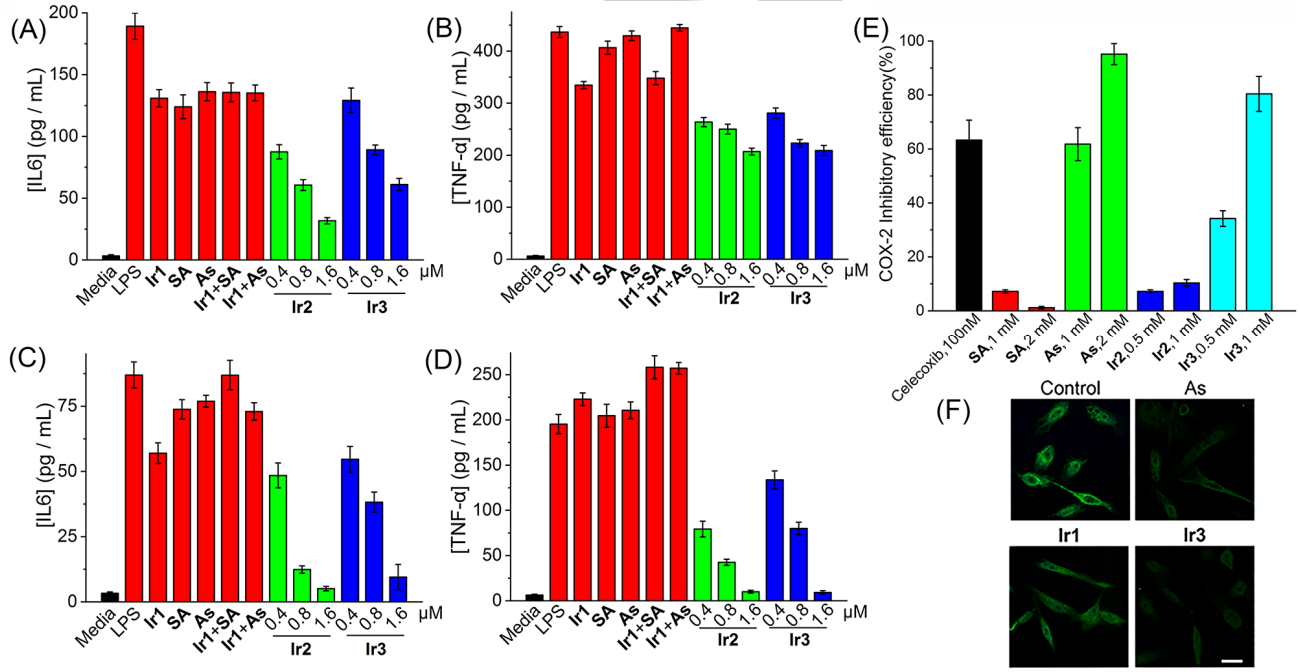

Figure 2. (A–D) Anti-inflammatory properties of Ir(III) complexes. The effects of **Ir2**, **Ir3**, **As**, **SA**, and mixtures of **Ir1** with **As**/**SA** at molar ratio of 1:2 on the levels of IL-6 and TNF-*α* in RAW 264.7 macrophages assessed by ELISA. (A and B) The cells were pretreated with LPS (100 ng/mL, 6 h) and then incubated with tested compounds at the indicated doses for 12 hours. The concentration not mentioned in the figure is the highest dose of **Ir2** and **Ir3**. (C and D) The cells were incubated with test compounds for 6 hours and further treated with LPS (100 ng/mL, 12 h). The concentration not mentioned in the figure is the highest dose of **Ir2** and **Ir3**. (E) Inhibition of human COX-2 by Celecoxib (100 nM), **As** (1 mM, 2 mM), **SA** (1 mM, 2 mM), **Ir2** (0.5 mM, 1 mM) and **Ir3** (0.5 mM, 1 mM) *in vitro*. (F) Impact of **Ir1** (2 μM), **Ir3** (2 μM) and **As** (4 μM) on the expression of COX-2 in PC3 cells analyzed by immunofluorescence staining. Scale bar: 10 μm.

10.1002/chem.201900851

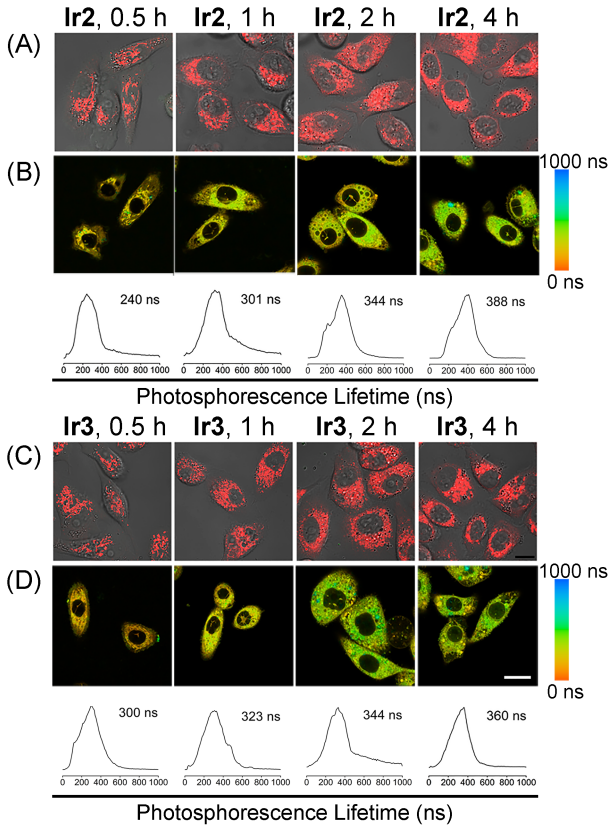

Figure 3. Real-time tracking of the mitochondrial morphology by **Ir2** (10 μM, A) and **Ir3** (10 μM, C) monitored by confocal microscopy over a period of 4 h. λ_{ex} = 405 nm; λ_{em} = 600 ± 20 nm. PLIM images of PC3 cells incubated with **Ir2** (10 μM, B) and **Ir3** (10 μM, D). λ_{ex} = 405 nm; λ_{em} = 600 ± 20 nm. Scale bar: 20 μm.

Mitochondrial Real-Time Tracking and Lifetime Imaging

The log $P_{o/w}$ values, representing the lipophilicity of the drug, of **Ir1** (0.21), **Ir2** (0.70) and **Ir3** (1.01) are determined by a shake-flask method. After an incubation at 10 μM for 1 h, inductively coupled plasma-mass spectrometry (ICP-MS) measurement shows that the cellular uptake levels of **Ir1**, **Ir2** and **Ir3** are 0.22, 2.00 and 2.18 ng per μg protein, respectively. The results indicate that the conjugation elevates the lipophilicity of the complexes, thereby increases their uptake efficiency and cytotoxicity. The emission of **Ir2** and **Ir3** in cells incubated at 4 °C or pretreated with carbonyl cyanide m-chlorophenyl hydrazone (CCCP) is weaker than that incubated at 37 °C (Figure S17). However, chloroquine doesn't show obvious effect on the uptake of **Ir2** and **Ir3**. The results indicate that **Ir2** and **Ir3** enter cells mainly by an energy-dependent mechanism instead of endocytosis.

Confocal microscopy experiment shows that **Ir2** (10 μM) and **Ir3** (10 μM) can effectively enter PC3 cells after an incubation for 1 h (Figure S18). **Ir2** and **Ir3** are mainly scattered in cytoplasm. Both **Ir2** and **Ir3** can overlap with MitoTracker Deep Red (MTDR, Figure S19A), indicating that **Ir2** and **Ir3** can locate in mitochondria specifically. The pearson's colocalization coefficients of **Ir2** and **Ir3** with MTDR are 0.84 and 0.86, respectively, while little overlap is found for **Ir2**/**Ir3** with LysoTracker Deep Red (LTDR, Figure S19B). As measured by ICP-MS, the content of iridium in mitochondria is higher than that in cytoplasm and nucleus (Figure S19C), indicating that both **Ir2** and **Ir3** can accumulate in mitochondria.

The morphology of the mitochondria can reflect the status of the mitochondria.[44] Real-time tracking of the mitochondrial morphology was carried out by monitoring the emission of **Ir2** and **Ir3** in PC3 cells using confocal microscopy. PC3 cells can be effectively labelled by **Ir2** and **Ir3** after 0.5 h incubation, when mitochondria show the normal tubular network and distribution. As the incubation time increases, the normal tubular mitochondrial network turns into swelling mitochondrial aggregates, large perinuclear clusters (Figure 3 A and C).

Since iridium complexes have environmental-sensitive long phosphorescence lifetimes, time-gate imaging can be used to reduce the interference the background fluorescence.[14] More importantly, PLIM technology is very advantageous for phosphorescent metal complexes to accurately reflect the changes in the microenvironments.[45-46] After 4 h of treatment, the cellular lifetimes of **Ir2** and **Ir3** increase gradually (Figure 3B and D). The lifetime of **Ir2** changes from 240 ns to 388 ns, while that of **Ir3** changes from 300 ns to 360 ns. Because the complexes could go through hydrolysis in cells, we first studied the effect of hydrolysis on the lifetimes of **Ir2** and **Ir3**. After treatment with the hydrolase, the lifetime of **Ir2** decreases from 393 ns to 142 ns, while that of **Ir3** decreases from 631 ns to 249 ns (Figure S20). Therefore, hydrolysis is not the reason for the time-dependent increase in the lifetimes of Ir(III) in cells. During the process of mitochondrial damage, the polarity and other physical properties of mitochondria will change significantly.[47] Therefore, we studied the lifetimes of complexes in solvents of different polarities. The lifetimes of **Ir2** and **Ir3** are indeed affected by polarity, but no clear correlation is detected. The lifetime ($\tau_0(CH_3CN) < \tau_0(DMSO) < \tau_0(CH_2Cl_2)$) does not increase with the increase of polarity (CH_2Cl_2 < CH_3CN < DMSO, Figure S21). Finally, we speculate that the increase in the lifetimes of complexes in cells may be due to the aggregation of complexes. It has been reported that the fluorescence intensities and lifetimes of iridium complexes can be significantly influenced by the aggregation states.[48-50] As in the solid state, the complexes show relatively longer lifetimes (Table S1). Moreover, with the increase of the aggregation degree of complexes, their lifetimes tend to increase (Figure S22). Therefore, we reckon that the changes in the aggregation state of the complexes in mitochondria lead to the increase in the lifetimes of complexes in cells.

Induction Mitochondrial Dysfunction and Metabolic Disorders

As **Ir2** and **Ir3** located in mitochondria, the influence on mitochondria integrity was then monitored by detecting the

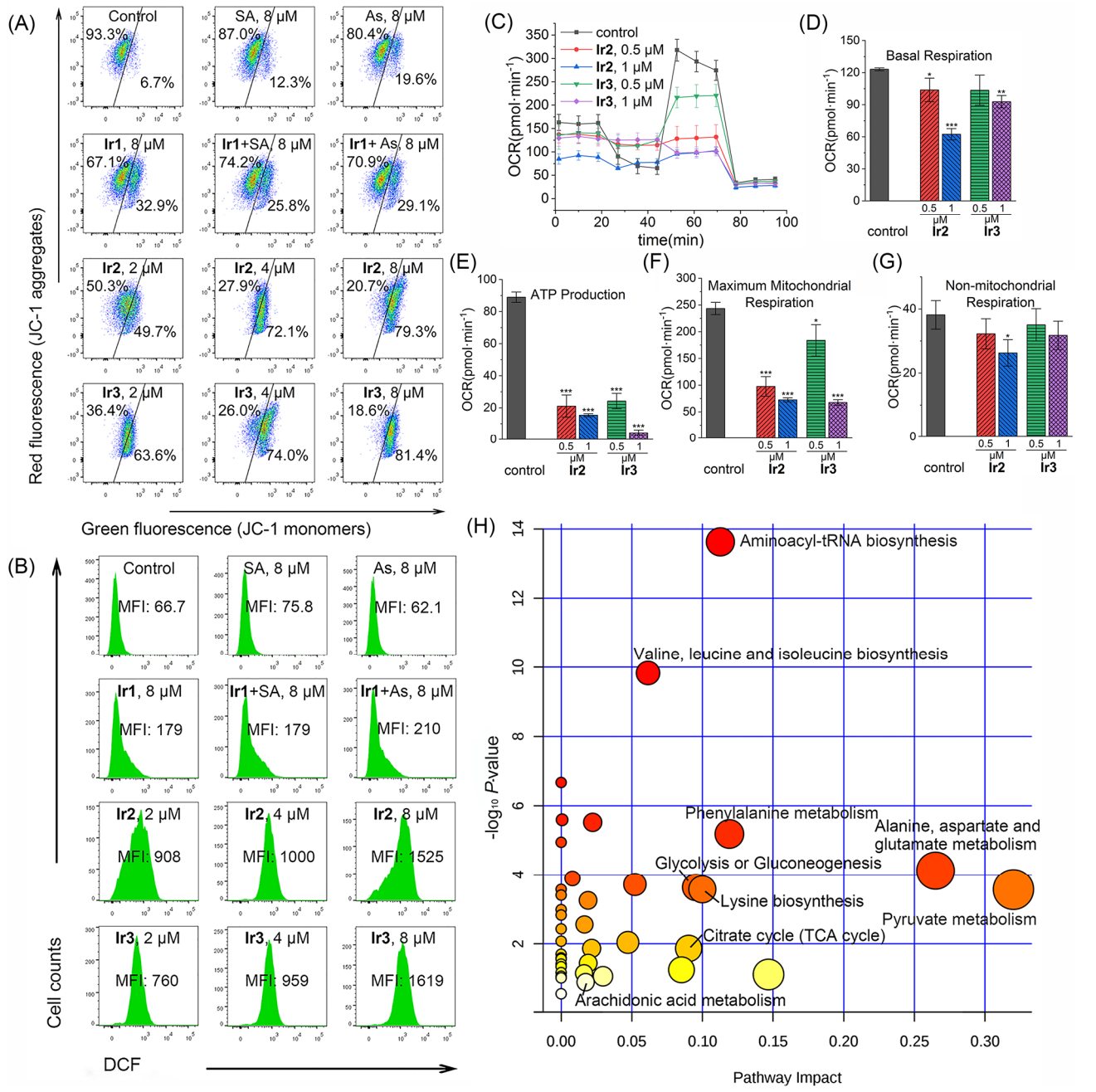

Figure 4. (A) Detection of MMP stained with JC-1 on flow cytometry. λ_{ex} = 488 nm. λ_{em} = 530 ± 30 nm and 585 ± 30 nm. (B) Intracellular ROS generation detected by DCF (λ_{ex} = 488 nm; λ_{em} = 530 ± 30 nm) with flow cytometry. For (A) and (B), PC3 cells were treated with vehicle (1% dimethyl sulfoxide (DMSO)), **As**, **SA**, **Ir1**, mixtures containing **Ir1** and two-fold molar ratio of **As** or **SA**, **Ir2** or **Ir3** in the mentioned concentrations for 6 h. (C) Respiratory curves of control, **Ir2**- and **Ir3**-treated PC3 cells under basal conditions, and after the addition of oligomycin (1 mM), FCCP (0.8 mM) and the mixture of rotenone (0.5 mM) and antimycin A (0.5 mM) were recorded by a Seahorse XF24 extracellular flux analyzer. (D) Basal respiration was computed by subtracting OCR values after adding rotenone/antimycin A from basal OCR. (E) ATP production was computed by subtracting OCR values after adding oligomycin from basal OCR. (F) Maximum mitochondrial respiration was computed by subtracting OCR values after adding rotenone/antimycin A from the OCR values after the adding FCCP. (G) Non-mitochondrial respiration was the OCR value after adding rotenone/antimycin A. *p < 0.05, **p < 0.01, ***p < 0.001, compared with control. (H) Summary of metabolic pathway analysis of PC3 cells treated with **Ir3**. The color of the circles means the pathway impact, and the area of the circles means p-value.

changes of mitochondrial membrane potential (MMP) using 5,5',6,6'-tetrachloro-1,1'-3,3'-tetraethyl-benzimidazolylcarbocyanine iodide (JC-1) staining. A concentration-dependent reduction in MMP can be found in **Ir2**- and **Ir3**-treated cells (Figure 4A). After 6 h treatment, the proportion of cells with depolarized mitochondria increase from 6.7% (control) to 79.3% and 81.4% for **Ir2** (8 μM) and **Ir3** (8 μM), respectively. The ability of these complexes to depolarize

mitochondria correlates with their cytotoxicity. The impact of **Ir1** in combination of 2-fold of **As** or **SA** on MMP is much lower than the corresponding conjugates.

To further investigate the effects of **Ir2** and **Ir3** on mitochondrial energetics, the intracellular ATP levels were measured. Compared with the control, **Ir2** and **Ir3** treatment causes dose-dependent declines in ATP levels (Figure S23). At a concentration of 8 μM, the ATP levels decrease by about 46.8% and 47.6 % for **Ir2** and **Ir3**, respectively.

The increase of intracellular ROS levels caused by **Ir2** and **Ir3** were then measured by the 2′,7′-dichlorodihydrofluorescein diacetate (H_2DCF-DA) staining assay. After treated with **Ir2** and **Ir3**, the cellular ROS levels are increased obviously (Figure 4B). The emission of DCF increases by about 22.9-fold and 24.3-fold in cells incubated with **Ir2** (8 μM, 6 h) and **Ir3** (8 μM, 6 h), respectively.

We also evaluated the effect of **Ir2** and **Ir3** on mitochondrial respiration by measuring the oxygen consumption rate (OCR). Several key parameters were measured to assess mitochondrial oxidative phosphorylation (OXPHOS)[51] by using respiration modulators targeting electron transport chain components (Figure 4C). Compared with control, cells treated with **Ir2** and **Ir3** show a concentration-dependent decrease in basal respiration (Figure 4D), ATP production (Figure 4E), and maximal respiration (Figure 4F). A slight decrease is also founded in non-mitochondrial respiration (Figure 4G). These results imply that **Ir2** and **Ir3** can damage the mitochondrial bioenergetic functions by interfering with the mitochondrial respiration.

Cancer cells are reported to have altered or dysfunctional mitochondrial metabolism.[52] The impact of **Ir2** and **Ir3** on mitochondrial metabolism was investigated. The metabolites of PC3 cells treated with **Ir2** or **Ir3** were extracted with methanol and chloroform and analyzed by GC-TOF-MS (Gas Chromatography Time-of-Flight Mass Spectrometry). The data were analyzed using PCA (principal component analysis) to find outliers (Figure S24). Then, candidate biomarkers were picked out from S-plots following analysis of OPLS-DA (orthogonal projections to latent structures discriminant analysis). The OPLS-DA score plots for the **Ir2-**treated samples and controls are shown in Figure S25. The R^2Y (the goodness of fit) and Q^2Y (predictability) values are 0.989 and 0.91, respectively. The cluster of the **Ir2-**treated group is located far away from that of the controls, which indicates that the metabolic profile of **Ir2**-treated samples is different from that of the controls. Similarly, the OPLS-DA score plots of **Ir3**-treated samples and controls (Figure S27, R^2Y = 1, Q^2Y = 0.98) show a clear discrimination. The S-plots are shown in Figure S26 and S28. To find potential biomarkers, 18 potential biomarkers (Table S2) between **Ir2**-treated group and control group with the VIP >1 and *p*-value <0.05 were selected for further analysis. Similarly, the 22 potential biomarkers (Table S3) between **Ir3**-treated group and control group were selected for further analysis. To explore the potential metabolic pathways, these metabolites were then analyzed by MetaboAnalyst (Figure 4H and Figure S29). **Ir3**-treated cells exhibit aberrant levels of pyruvate metabolites (elevation of pyruvate and reduction of lactate) that is associated with glycolysis/gluconeogenesis. **Ir3** also impairs the amino acids metabolism, causing the accumulation of valine, leucine, isoleucine, phenylalanine, lysine, aspartate and tyrosine. Similar result is found in **Ir2**-treated samples. **Ir2**-treated cells showed accumulation of pyruvate and citrate cycle metabolites, pyruvate, citrate and malate. **Ir2** impairs the amino acids metabolism, causing the accumulation of glycine, valine, leucine, isoleucine, threonine, serine, tyrosine and lysine. The result indicates that **Ir2** and **Ir3** can impair mitochondrial biosynthesis leading to mitochondrial dysfunction.

Induction of Caspase-Dependent Apoptosis and Caspase-Independent Paraptosis

Based on morphological and biochemical criteria, cell death can be divided into many categories, e.g., apoptosis, necrosis, autophagy and paraptosis.[53] The morphological changes in Ir(III)-treated cells were first analyzed by transmission electron microscopy (TEM) (Figure 5A). Extensive cytoplasmic vacuolation, widening of the membrane space with intact nucleus are observed in cells treated with **Ir2** and **Ir3** at a lower dose (2 μM). These morphological changes are the typical paraptosis symptoms.[54] However, cells treated with **Ir2** and **Ir3** at a higher concentration (8 μM) display typical characteristics of apoptosis including chromatin condensation and nuclear fragmentation[55].

2'-(4-ethoxyphenyl)-5-(4-methyl-1-piperazinyl)-1H,3'H-2,5'-bibenzimidazole (Hoechst 33342) staining doesn't show obvious change in cell nuclei after **Ir2**- or **Ir3**-treatment at a relatively lower concentration (2 μM) in PC3 cells, but typical apoptotic alternations are observed in cells treated at a higher dose (8 μM) (Figure 5B). Apoptosis is usually caspase-dependent while paraptosis often occurs in the caspase-independent pathway.[56] Compared with the control, little change of caspase-3/7 activity is found in cells treated with **Ir2** or **Ir3** at 2 μM (Figure 5C). However, the activity of caspase-3/7 is increased by approximately 4.2- and 8.5-fold in **Ir2**- and **Ir3**-treated cells at 8 μM, respectively.

In order to further verify the cell death modes induced by **Ir2** and **Ir3**, we studied the effect of different cell death inhibitors on cell viability. Pretreatment of the pan-caspase inhibitor z-VAD-fmk (50 μM) increases the cell viability for **Ir2** (8 μM) and **Ir3** (8 μM) treatment (Figure 5D). Treated with cycloheximide, an inhibitor associated with paraptosis,[52] can effectively diminish the cell death induced by **Ir2** and **Ir3** at a low concentration (2 μM) (Figure 5E). But cycloheximide fails to protect cells from the cytotoxic effects of **Ir2** and **Ir3** at a relatively higher concentration (8 μM). The possibilities of autophagy and necrosis are excluded based on the fact that 3-MA (3-methyladenine, an autophagy inhibitor) and Nec-1 (a RIP1-specific inhibitor that can prevent necrosis) show no obvious effects on both **Ir2**- and **Ir3**-induced cell death (Figure S30 and S31). These results imply that **Ir2** and **Ir3** can induce caspase-independent paraptosis and caspase-dependent apoptosis at lower and higher concentrations, respectively.

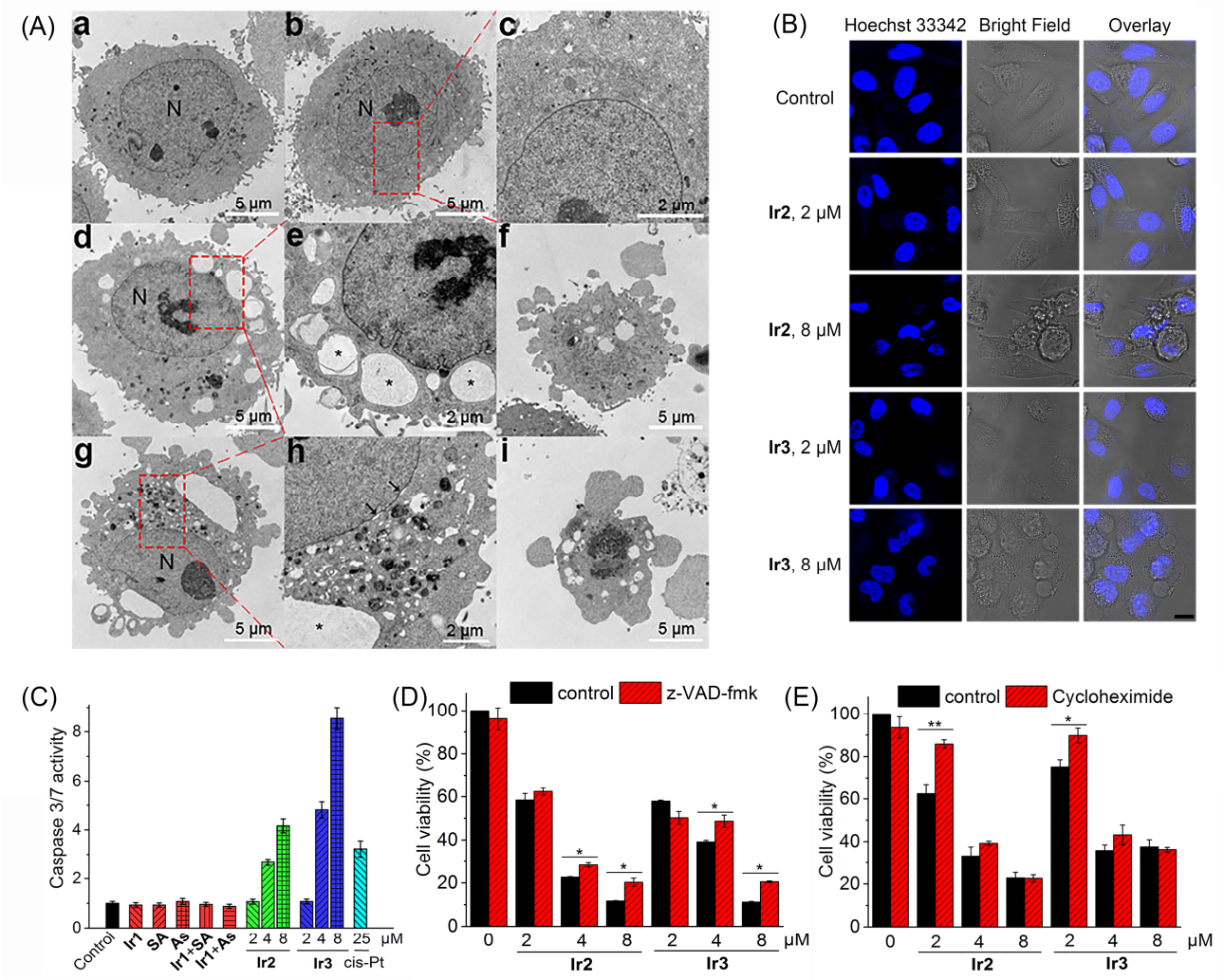

Figure 5. (A) TEM graphs of PC3 cells treated with **Ir2** and **Ir3** at the indicated doses for 24 hours. PC3 cells were treated with vehicle (a), **Ir1** (10 μM, b and c), **Ir2** (4 μM, d and e), **Ir2** (8 μM, f), **Ir3** (4 μM, g and h) or **Ir3** (8 μM, i) for 24 h. Nuclei are labelled N. Black arrows: the nuclear membrane is affected, while the nucleus is intact. The red dotted box represents the enlarged area. (B) PC3 cells staining with Hoechst 33342 after treated with **Ir2** and **Ir3** at the indicated doses for 24 hours. (C) Caspase-3/7 activity in PC3 cells after incubated with **Ir2**, **Ir3** or cisplatin for 6 hours. (D) The effect of z-VAD-fmk on the cytotoxicity of **Ir2** and **Ir3**. PC3 cells were incubated with **Ir2** and **Ir3** at varying concentrations for 24 hours in the absence or presence of z-VAD-fmk. (E) The impact of cycloheximide on the cytotoxicity of **Ir2** and **Ir3**. *p< 0.05, **p< 0.01, as compared with the group without z-VAD-fmk or cycloheximide treatment.

Inhibition of Metastasis-Related Events

Cancer is a multistep and multifactorial process, and cancer cells are different from their normal counterparts in many aspects.[58] The effects of **Ir1**–**Ir3** on migration was measured by the wound healing assay and transwell assay. After 24 h incubation, **Ir1**–**Ir3** (0.5 μM) can effectively inhibit cell movement with a wound closure ratio of 3.1–4.6%, which is much lower as compared with that of the vehicle control (18.6%) (Figure 6A and 6C). Transwell assay shows that **Ir2** (0.5 μM) and **Ir3** (0.5 μM) decrease the cell migration ratios to 48.2% and 54.5% (the ratio of the vehicle control cells is counted as 100%), respectively (Figure 6B and 6D).

Then, we evaluated the capability of inhibiting colony formation by **Ir2** and **Ir3** at different concentrations. As shown in Figure 6E, after 48 h exposure, both **Ir2** and **Ir3** demonstrate a concentration-dependent anti-proliferative effect on colony formation. Colonies can be completely restrained after treated with **Ir2** or **Ir3** at 1 μM. The cytotoxic assay shows that the cell viability is not obviously affected at the concentration tested (Figure S32).

A tube formation assay was carried out to assess the anti-angiogenesis properties of the Ir(III) complexes

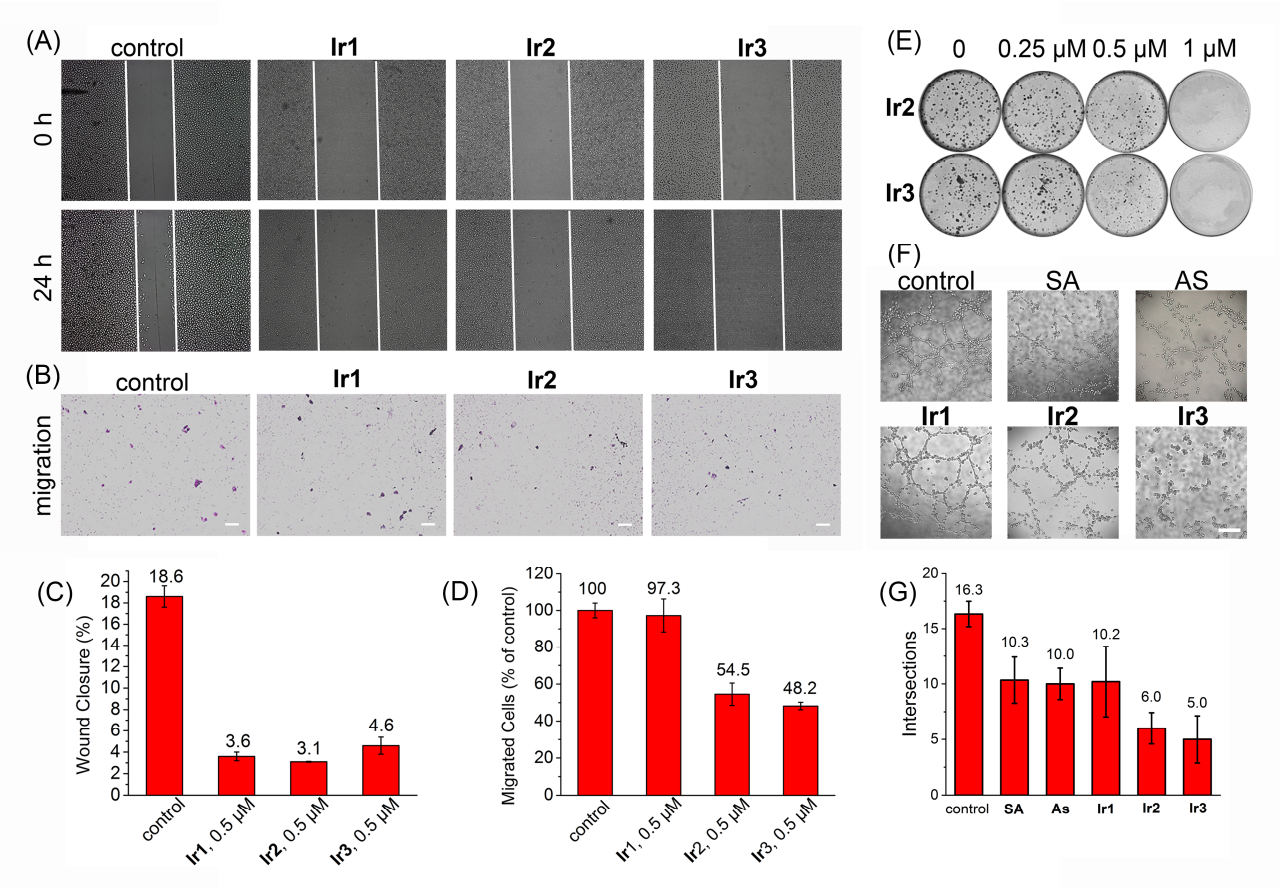

Figure 6. (A) Wound healing of PC3 cells after treated with **Ir1**–**Ir3** (0.5 μM) for 24 h. (B) Graphs of migrated cells. PC3 cells (1×10^5) were treated with **Ir1**–**Ir3** (0.5 μM) for 24 hours. Scale bars: 100 μm. (C) Wound closure rate. Wound closure (%) = [1 −(width at 24 h) /(width at 0 h)] × 100%. (D) Percentage of migrated cells compared with the control. (E) Inhibition of colony formation by **Ir2** and **Ir3** at the indicated doses. PC3 cells were treated with **Ir2** and **Ir3** for 48 hours and further incubated for a week. (F) Effect of **Ir1**–**Ir3** against the tube formation of HUVEC on matrigel. HUVEC seeded on matrigel in medium were treated with **As** (2 μM), **SA** (2 μM), **Ir1** (1 μM), **Ir2** (1 μM) or **Ir3** (1 μM) for 4 h. scale bar : 200 μm. (G) Quantification of tube formation or intersections between cells counted manually.

(Figure 6F and 6G).Human umbilical vein endothelial cells (HUVEC) can connect as network after plated on the matrix. Compared with the control cells, much less tubes are formed and the network disappears in Ir(III)-treated samples. MTT assay shows that the compounds has low cytotoxicity at this concentration (Figure S33). Similar phenomena are also observed for **SA** and **As**, which is also consistent with the literature reports that anti-angiogenesis is involved in the anticancer properties of **As**.[59]

Inhibition of Tumor Xenografts Growth *In Vivo*

To evaluate the antitumor effects of **Ir2** and **Ir3** *in vivo*, we used PC3 cells to build subcutaneous tumor xenografts model in female BALB/c nude mice. As shown in Figure 7A and Figure 7B, tumor growth was significantly slowed in mice intraperitoneally injected with **Ir2** and **Ir3**, compared with the control group. After 21 days treatment, the tumor volume decreases by 44 ± 13% and 55 ± 7% for **Ir2**- and **Ir3**-treatment, respectively. Under the same conditions, the *in vivo* anticancer activity of **Ir2**/**Ir3** is approximate to that of cisplatin. No significant difference is found in body weight among all groups of mice (Figure 7C), which indicates **Ir2** and **Ir3** do not cause severe side effects in these conditions.

Conclusion

In this study, two Ir(III) complexes with a cyclometalated Ir(III) moiety for mitochondrial targeting and **As** or **SA** for immuno-modulating, linked through ester bonds have been synthesized. Conjugation of **SA** or **As** to the Ir(III) moiety can improve the cellular uptake efficacy of the Ir(III) complexes and achieve a high synergetic effect. Mechanism studies indicate that **Ir2** and **Ir3** accumulate in mitochondria and induce caspase-dependent apoptosis at lower doses and caspase-independent paraptosis at higher concentrations. Using PLIM techniques, we observed that **Ir2** and **Ir3** aggregate in the mitochondria over time. As

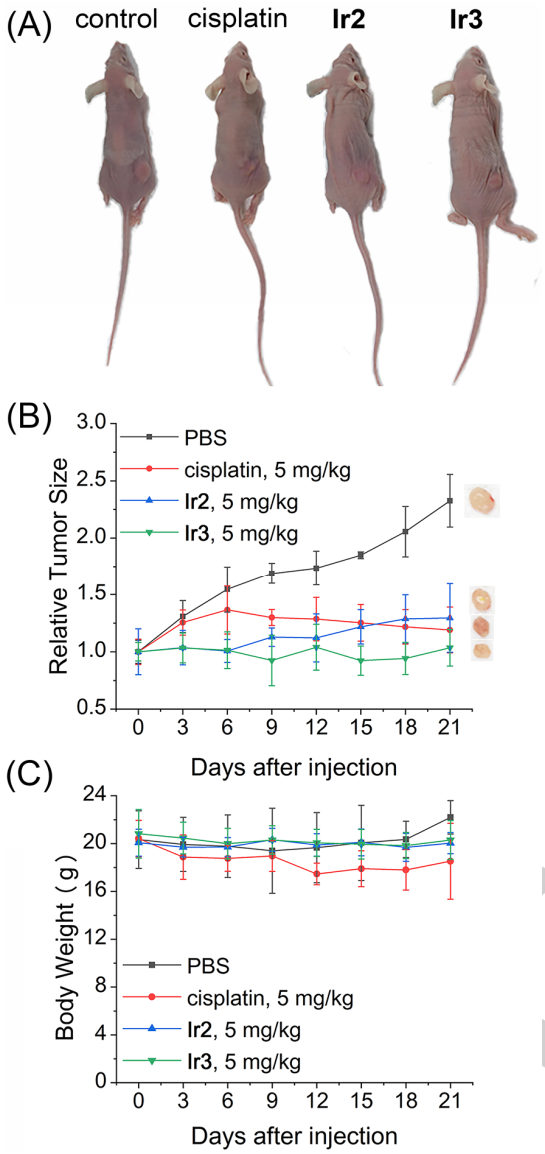

Figure 7. Representative graphs of nude mice (A) after 21 days treated with PBS, **Ir2**, **Ir3** and cisplatin. Growth curve of tumor volume (B) and body weight of mice (C) after intraperitoneal injection of PBS, **Ir2**, **Ir3** and cisplatin.

expected, they exhibit immunomodulatory properties by regulating the activity of some immune factors and inhibiting COX-2. Moreover, they can inhibit migration, colony-formation and angiogenesis. *In vivo* experiments also show that **Ir2** and **Ir3** show potent growth inhibitory effect on human solid tumor and low systemic toxicity. Our study shows that a joint action of mitochondrial targeting with immuno-modulating anticancer strategies is a feasible strategy to develop metalloanticancer agents with multiple anticancer effects.

Experimental Section

Materials and Measurements

$IrCl_3 \cdot nH_2O$, ppy, DMF, **SA**, **As**, NH_4PF_6 were purchased from Alfa Aesar (USA). **L1** was purchased from TCI (China). Cisplatin, DMSO, MTT, Hoechst 33342 and H_2DCF-DA were purchased from Sigma Aldrich (USA). MTDR, LTDR, and JC-1 were obtained from Life Technologies (USA). LPS was purchased from Invitrogen (USA). Primary rabbit polyclonal antibody for COX-2 and Alexa Fluor® 488 goat anti-rabbit secondary antibody were purchased from Abcam (USA). Cellular ATP quantification assay kit and caspase-3/7 activity kit were purchased from Promega (USA). TNF-α and IL-6 were tested using eBiosciences ELISA-Ready-Set Go® (USA).

ESI-MS was recorded on a Thermo Finnigan LCQ DECA XP spectrometer (USA). NMR spectra were recorded on a Bruker Avance III 400 MHz spectrometer or a Bruker Avance III 500 MHz spectrometer. Elements analysis (C, H, and N) was done by an Elemental Vario EL CHNS analyzer. UV/Vis spectra were conducted on a Varian Cary 300 spectrophotometer. Emission spectra and lifetimes were measured by a fluorescence spectrometer (FLS 920, Edinburgh Instruments Ltd). Cell imaging experiments were performed by a confocal microscope (LSM 710, Carl Zeiss, Göttingen). Flow cytometry was carried out by a BD FACS Calibur™ flow cytometer (Becton Dickinson).

Synthesis and Characterization

4,4'-bis(bromomethyl)-2,2'-bipyridine. 4,4'-bis(bromomethyl)-2,2'-bipyridine was prepared according to the literature method [60]. 4,4'-bis(hydroxymethyl)-2,2'-bipyridine (4 g, 11.7 mmol) was dissolved in a mixture of HBr (48%, 30 mL) and concentrated H_2SO_4 (10 mL). The resulting solution was refluxed for 6 h and allowed to cool, and water (100 mL) was added. The pH was adjusted to 7.0 by the addition of NaOH saturated solution, and the resulting precipitate was filtered, washed with water, and air-dried.

General procedures for the preparation of L2 and L3. 2 mmol phenolic acid was dissolved in 3 mL dry DMF, and 2.4 mmol $KHCO_3$ was added and stirred for several minutes at room temperature. Then, 4,4'-bis(bromomethyl)-2,2'-bipyridine (342 mg, 1 mmol) were added. The reaction mixture was stirred for 6 h at room temperature. The reaction mixture was added to 10 mL water and extracted with ethyl acetate. The organic layer was subsequently washed with 5% $NaHCO_3$ and 5% NaCl, dried over anhydrous Na_2SO_4, filtered and concentrated under reduced pressure to give the desired products.

[2,2'-bipyridine]-4,4'-diylbis(methylene) bis(2-hydroxybenzoate) (L2): **L2** was obtained as a white solid. Yield: 415 mg (91%). ^{1}H NMR (400 MHz, $CDCl_3$) δ 10.58 (s, 2H, OH-1), 8.72 (d, *J* = 5.0 Hz, 2H, CH-2), 8.50 (s, 2H, CH-3), 7.95 (dd, *J* = 8.0, 1.5 Hz, 2H, CH-4), 7.55–7.46 (m, 2H,CH-5), 7.40 (d, *J* = 4.5 Hz, 2H, CH-6), 7.01 (d, *J* = 8.4 Hz, 2H, CH-7), 6.92 (t, *J* = 7.6 Hz, 2H, CH-8), 5.49 (s, 4H, CH2-9). ESI-MS (CH_3OH): m/z 457.6 $[M+H]^+$. Elemental analysis calcd (%) for $C_{26}H_{20}N_2O_6 \cdot 0.25\ H_2O$: C 67.75, H 4.48, N 6.08; found: C 67.73, H 4.69, N 6.28.

[2,2'-bipyridine]-4,4'-diylbis(methylene) bis(2-acetoxybenzoate) (L3): **L3** was obtained as a white solid. Yield: 459 mg (85%). ^{1}H NMR (500 MHz, $CDCl_3$) δ 8.71 (d, *J* = 5.0 Hz, 2H, CH-1), 8.47 (s, 2H, CH-2), 8.12 (dd, *J* = 7.9, 1.6 Hz, 2H, CH-3), 7.60 (td, *J* = 7.8, 1.6 Hz, 2H, CH-4), 7.38 (dd, *J* = 4.9, 0.8 Hz, 2H, CH-5), 7.37 – 7.32 (m, 2H, CH-6), 7.13 (d, *J* = 8.0 Hz, 2H, CH-7), 5.42 (s, 4H, CH_2-8), 2.26 (s, 6H, CH_3-9). ESI-MS (CH_3OH): m/z 541.4 $[M+H]^+$. Elemental analysis calcd (%) for $C_{30}H_{24}N_2O_8 \cdot 0.8\ CH_3OH$: C 65.34, H 4.84, N 4.95; found: C 65.93, H 4.94, N 5.14.

Synthesis of Ir1–Ir3. The dimeric iridium(III) precursors $[Ir(ppy)_2(\mu\text{-}Cl)]_2$ were prepared according to the literature method. Complex **Ir1** was synthesized according to the literature methods [35]. Complexes **Ir2** and **Ir3** were synthesized similarly. A mixture of $[Ir(ppy)_2(\mu\text{-}Cl)]_2$ (0.2 mmol) and **L2** (0.4 mmol) or **L3** (0.4 mmol) in CH_2Cl_2/CH_3OH (1:1, v/v) was heated to reflux under the protection by nitrogen in the dark for 6 h. The solution was cooled to room temperature and evaporated to dryness under reduced pressure. The oil-like substance was dissolved in CH_2Cl_2 and purified by column chromatography on silica gel eluted with CH_2Cl_2/CH_3OH. A 4-fold excess of NH_4PF_6 was added into the solution and stirred for 1 h. The mixture was filtered and the filtrate was evaporated under reduced pressure to obtain dry powder. The crude product was washed with water to remove excess NH_4PF_6. The desired product was further purified by recrystallization.

$[Ir(ppy)_2(L2)](PF_6)$ (Ir2): **Ir2** was obtained as an orange red solid. Yield: 335 mg (76%). ^{1}H NMR (500 MHz, [d_6]-DMSO) δ 10.39 (s, 2H, OH-1), 8.96 (s, 2H,CH-2), 8.27 (d, *J* = 8.2 Hz, 2H, CH-3), 7.98 – 7.91 (m, 6H, CH-4), 7.90 (d, *J* = 5.7 Hz, 2H, CH-5), 7.86 (d, *J* = 5.4 Hz, 2H, CH-6), 7.69 (d, *J* = 5.6 Hz, 2H), 7.57 – 7.50 (m, 2H), 7.17 (t, *J* = 6.2 Hz, 2H), 7.06 – 6.98 (m, 4H), 6.96 – 6.88 (m, 4H, CH-11), 6.21 (d, *J* = 7.5 Hz, 2H, CH-12), 5.63 (s, 4H, CH_2-13). ESI-MS (CH_3OH): m/z 957.5 $[M-PF_6]^+$. Elemental analysis calcd (%) for $C_{48}H_{36}F_6IrN_4O_6P•H_2O$: C 51.47, H 3.42, N 5.00; found: C 51.30, H 3.31, N 5.03.

$[Ir(ppy)_2(L3)](PF_6)$ (Ir3): **Ir3** was obtained as a bright yellow solid. Yield: 323 mg (68%). ESI-MS (CH_3OH): m/z 1041.4 $[M-PF_6]^+$. ^{1}H NMR (400 MHz, [d_6]-DMSO) δ 8.90 (s, 2H), 8.28 (d, *J* = 8.2 Hz, 2H), 8.11 – 8.08 (m, 2H), 7.94 (d, *J* = 8.0 Hz, 4H), 7.89 (d, *J* = 5.7 Hz, 2H), 7.82 – 7.79 (m, 2H), 7.79 – 7.69 (m, 4H), 7.68 (d, *J* = 5.8 Hz, 2H), 7.41 (td, *J* = 7.7, 1.1 Hz, 2H), 7.26 (dd, *J* = 8.1, 0.9 Hz, 2H), 7.19 – 7.14 (m, 2H), 7.06 – 7.00 (m, 2H), 6.92 (td, *J* = 7.4, 1.1 Hz, 2H), 6.20 (d, *J* = 6.8 Hz, 2H), 5.53 (s, 4H), 2.10 (s, 6H).Elemental analysis calcd (%) for $C_{53}H_{43}F_6IrN_4O_8P$: C 53.00, H 3.61, N 4.66; found: C 52.96, H 3.64, N 4.57.

Hydrolysis of Ir2 and Ir3 by PLE *In Vitro*

Time-dependent emission spectra and Luminescence decay signals. **Ir2** and **Ir3** (20 μM) in degassed PBS were freshly prepared and added into quartz cuvettes (3 mL), and then PLE (1 μL) in $(NH_4)_2SO_4$ suspension was sequentially added. For each time, the emission spectra were recorded after 5 min incubation of the reaction mixture at 310 K. The luminescence decay curves were recorded for the indicated time intervals.

ESI-MS. Ir(III) solutions (20 μM, 3 mL) in degassed PBS were freshly prepared and PLE (1 μL) was added. The samples were analyzed by ESI-MS after incubation at 310 K for different time intervals.

Cell Lines and Culture Conditions

PC3, HT29, CT26, RAW 264.7 and HUVEC were purchased from Experimental Animal Center of Sun Yat-Sen University (Guangzhou, China). Cells were cultured with ATCC recommended media. The cells were maintained in tissue culture flasks in an incubator at 37 °C under 5% CO2.

Cytotoxicity Assay

The cytotoxicity of the compounds was measured as previously described [61]. When necessary, cells were pretreated with cycloheximide (1 μM), z-VAD-fmk (50 μM), 3-MA (1 mM) or Nec-1 (100 μM) for an hour before **Ir2** and **Ir3** were added. Each experiment was repeated at least three times to gain the mean values.

Anti-Inflammatory Properties by ELISA

RAW 264.7 cells were seeded in 96-well plates and allowed to grow overnight. For the preventative anti-inflammatory treatment, RAW cells were treated with **Ir1** (10 μM), **As** (10 μM), **SA** (10 μM), mixtures containing **Ir1** (10 μM) and **As** (20 μM)/**SA** (20 μM), **Ir2** (0.4, 0.8 or 1.6 μM), and **Ir3** (0.4, 0.8 or 1.6 μM) for 6 hours. The cells were treated with LPS (100 ng/mL) for another 12 hours. For the therapeutic anti-inflammatory treatment, the cells were treated with LPS (100 ng/mL) for 6 hours. **Ir1** (10 μM), **As** (10 μM), **SA** (10 μM), mixtures containing **Ir1** (10 μM) and **As** (20 μM)/**SA** (20 μM), **Ir2** (0.4, 0.8 or 1.6 μM), and **Ir3** (0.4, 0.8 or 1.6 μM) were then added and incubated for 12 hours. ELISA was performed on the supernatants against interleukin IL-6 and TNF-*α*, according to the manufacturer's instructions.

Mitochondrial Bioenergetics Analysis

The experiment was carried out as literature mentioned [35]. PC3 cells were seeded 2 × 10^4 per well. The optimal concentrations of the compounds were as following: oligomycin (1 μM), FCCP (0.8 μM) and a mixture of antimycin A (0.5 μM) and rotenone (0.5 μM).

Metabolomics Analysis

Sample preparation: PC3 cells were plated in 15 cm dishes (Corning) and cultured for 24 hours. After incubated with **Ir2** and **Ir3** for 6 hours, the PC3 cells were trypsinised, washed 3 times with PBS and counted. The centrifuged cell pellets were soaked in liquid nitrogen for at least 3 min then stored at −80 °C before test.

Metabolites extraction : The sample were transferred to 2 mL EP tubes and extracted with 1 mL extraction solvent ($V_{Methanol}$:$V_{Chloroform}$ = 3:1). 5 μL of adonitol (internal standard, 0.5 mg/mL in dH_2O) was then added.

GC-TOF-MS analysis : GC-TOF-MS analysis was done according to literature conditions.[62]

Data processing and annotation: Peaks were exacted using Chroma TOF 4.3X software and LECO-Fiehn Rtx5 database.[62]

Statistical analysis: Statistical analysis was performed by SIMCA-P 14.1 software. PCA was carried out to detect trends, and groupings. The data were analyzed by orthogonal partial least squares (OPLS). The variables with variable importance projection (VIP) > 1 in OPLS-DA score plots were usually regarded as candidate biomarkers. Metabolism pathways were noted by the Kyoto Encyclopedia of Genes and Genomes (KEGG) database. Pathway enrichment analysis was conducted with MetaboAnalyst.

Acknowledgements

This study was supported by the National Natural Science Foundation of China (21778078, 21837006, 21571196 and 21572282), the 973 program (2015CB856301), the Guangdong Natural Science Foundation (2015A030306023), the Innovative Research Team in University of Ministry of Education of China

(IRT_17R111) and the Fundamental Research Funds for the Central Universities.

Keywords: iridium complexes • aspirin • anticancer • mitochondrion • immunomodulation

[1] E. R. Jamieson, S. J. Lippard, *Chem. Rev.* **1999**, *99*, 2467-2498.
[2] G. Gasser, N. Metzler-Nolte, *Curr. Opin. Chem. Biol.* **2012**, *16*, 84-91.
[3] Z. Liu, P. J. Sadler, *Acc. Chem. Res.* **2014**, *47*, 1174-1185.
[4] A. Zamora, G. Vigueras, V. Rodriguez, M. D. Santana, J. Ruiz, *Coord. Chem. Rev.* **2018**, *360*, 34-76.
[5] W. Wang, C. Yang, S. Lin, K. Vellaisamy, G. Li, W. Tan, C. H. Leung, D. L. Ma, *Chem. Eur. J.* **2017**, *23*, 4929-4935.
[6] C. H. Leung, H. J. Zhong, H. Yang, Z. Cheng, D. S. Chan, V. P. Ma, R. Abagyan, C. Y. Wong, D. L. Ma, *Angew. Chem. Int. Ed.* **2012**, *51*, 9010-9014; *Angew. Chem.* **2012**, *124*, 9144-9148.
[7] L. J. Liu, W. Wang, Z. Zhong, S. Lin, L. Lu, Y. T. Wang, D. L. Ma, C. H. Leung, *Chem. Commun.* **2016**, *52*, 12278-12281.
[8] T. S. Kang, Z. Mao, C. T. Ng, M. Wang, W. Wang, C. Wang, S. M. Lee, Y. Wang, C. H. Leung, D. L. Ma, *J. Med. Chem.* **2016**, *59*, 4026-4031.
[9] C. H. Leung, S. Lin, H. J. Zhong, D. L. Ma, *Chem. Sci.* **2015**, *6*, 871-884.
[10] C. Y. Li, M. X. Yu, Y. Sun, Y. Q. Wu, C. H. Huang, F. Y. Li, *J. Am. Chem. Soc.* **2011**, *133*, 11231-11239.
[11] K. K. W. Lo, *Acc. Chem. Res.* **2015**, *48*, 2985-2995.
[12] H. F. Shi, H. B. Sun, H. R. Yang, S. J. Liu, G. Jenkins, W. Feng, F. Y. Li, Q. Zhao, B. Liu, W. Huang, *Adv. Funct. Mat.* **2013**, *23*, 3268-3276.
[13] Y. You, S. Lee, T. Kim, K. Ohkubo, W. S. Chae, S. Fukuzumi, G. J. Jhon, W. Nam, S. J. Lippard, *J. Am. Chem. Soc.* **2011**, *133*, 18328-18342.
[14] K. Y. Zhang, Q. Yu, H. J. Wei, S. J. Liu, Q. Zhao, W. Huang, *Chem. Rev.* **2018**, *118*, 1770-1839.
[15] Y. Chen, L. P. Qiao, L. N. A. Ji, H. Chao, *Biomaterials* **2014**, *35*, 2-13.
[16] Q. Zhao, C. Huang, F. Li, *Chem. Soc. Rev.* **2011**, *40*, 2508-2524.
[17] S. I. Grivennikov, F. R. Greten, M. Karin, *Cell* **2010**, *140*, 883-899.
[18] A. Jemal, R. Siegel, J. Q. Xu, E. Ward, *CA Cancer J. Clin.* **2010**, *60*, 277-300.
[19] J. Cuzick, F. Otto, J. A. Baron, P. H. Brown, J. Burn, P. Greenwald, J. Jankowski, C. La Vecchia, F. Meyskens, H. J. Senn, M. Thun, *Lancet Oncol.* **2009**, *10*, 501-507.
[20] P. M. Rothwell, F. G. R. Fowkes, J. F. F. Belch, H. Ogawa, C. P. Warlow, T. W. Meade, *Lancet* **2011**, *377*, 31-41.
[21] P. M. Rothwell, M. Wilson, C. E. Elwin, B. Norrving, A. Algra, C. P. Warlow, T. W. Meade, *Lancet* **2010**, *376*, 1741-1750.
[22] M. Michaud, I. Martins, A. Q. Sukkurwala, S. Adjemian, Y. T. Ma, P. Pellegatti, S. S. Shen, O. Kepp, M. Scoazec, G. Mignot, S. Rello-Varona, M. Tailler, L. Menger, E. Vacchelli, L. Galluzzi, F. Ghiringhelli, F. di Virgilio, L. Zitvogel, G. Kroemer, *Science* **2011**, *334*, 1573-1577.
[23] L. Zitvogel, L. Apetoh, F. Ghiringhelli, F. Andre, A. Tesniere, G. Kroemer, *J. Clin. Invest.* **2008**, *118*, 1991-2001.
[24] R. K. Pathak, S. Marrache, J. H. Choi, T. B. Berding, S. Dhar, *Angew. Chem. Int. Ed.* **2014**, *53*, 1963-1967; *Angew. Chem.* **2014**, *126*, 1994-1998.
[25] Q. Q. Cheng, H. D. Shi, H. X. Wang, Y. Z. Min, J. Wang, Y. Z. Liu, *Chem. Commun.* **2014**, *50*, 7427-7430.
[26] Q. Q. Cheng, H. D. Shi, H. X. Wang, J. Wang, Y. Z. Liu, *Metallomics* **2016**, *8*, 672-678.
[27] S. Fulda, L. Galluzzi, G. Kroemer, *Nat. Rev. Drug Discov.* **2010**, *9*, 447-464.
[28] G. Kroemer, *Oncogene* **2006**, *25*, 4630-4632.
[29] D. C. Wallace, *Nat. Rev. Cancer* **2012**, *12*, 685-698.
[30] S. E. Weinberg, N. S. Chandel, *Nat. Chem. Biol.* **2015**, *11*, 9-15.
[31] S. E. Weinberg, L. A. Sena, N. S. Chandel, *Immunity* **2015**, *42*, 406-417.
[32] S. M. McWhirter, B. R. tenOever, T. Maniatis, *Cell* **2005**, *122*, 645-647.
[33] L. A. Sena, S. Li, A. Jairaman, M. Prakriya, T. Ezponda, D. A. Hildeman, C. R. Wang, P. T. Schumacker, J. D. Licht, H. Perlman, P. J. Bryce, N. S. Chandel, *Immunity* **2013**, *38*, 225-236.
[34] E. L. Mills, B. Kelly, L. A. J. O'Neill, *Nat. Immunol.* **2017**, *18*, 488-498.
[35] J. J. Cao, C. P. Tan, M. H. Chen, N. Wu, D. Y. Yao, X. G. Liu, L. N. Ji, Z. W. Mao, *Chem. Sci.* **2017**, *8*, 631-640.
[36] A. T. Chan, S. Ogino, C. S. Fuchs, *New Engl. J. Med.* **2007**, *356*, 2131-2142.
[37] K. M. Kim, J. J. Song, J. Y. An, Y. T. Kwon, Y. J. Lee, *J. Bio. Chem.* **2005**, *280*, 41047-41056.
[38] W. W. Lin, M. Karin, *J. Clin. Invest.* **2007**, *117*, 1175-1183.
[39] K. Ishihara, T. Hirano, *Cytokine Growth F. R.* **2002**, *13*, 357-368.
[40] M. N. A. Khan, Y. S. Lee, *Med. Res. Rev.* **2011**, *31*, 161-201.
[41] A. J. Watson, *Histol. Histopathol.* **1998**, *13*, 591-597.
[42] J. A. Mitchell, P. Akarasereenont, C. Thiemermann, R. J. Flower, J. R. Vane, *Proc. Natl. Acad. Sci.* **1993**, *90*, 11693-11697.
[43] W. T. Godbey, A. Atala, *Gene Ther.* **2003**, *10*, 1519-1527.
[44] S. A. Detmer, D. C. Chan, *Nat. Rev. Mol. Cell Bio.* **2007**, *8*, 870-879.
[45] D. Y. Zhang, Y. Zheng, H. Zhang, J. H. Sun, C. P. Tan, L. He, W. Zhang, L. N. Ji, Z. W. Mao, *Adv. Sci.* **2018**, *5*, 1800581.
[46] L. Hao, Z. W. Li, D. Y. Zhang, L. He, W. T. Liu, J. Yang, C. P. Tan, L. N. Ji, Z. W. Mao, *Chem. Sci.* **2019**, *10*, 1285-1293.
[47] Z. Yang, Y. He, J. H. Lee, N. Park, M. Suh, W. S. Chae, J. Cao, X. Peng, H. Jung, C. Kang, J. S. Kim, *J. Am. Chem. Soc.* **2013**, *135*, 9181-9185.
[48] X. G. Hou, Y. Wu, H. T. Cao, H. Z. Sun, H. B. Li, G. G. Shan, Z. M. Su, *Chem. Commun.* **2014**, *50*, 6031-6034.
[49] Q. Zhao, L. Li, F. Li, M. Yu, Z. Liu, T. Yi, C. Huang, *Chem. Commun.* **2008**, 685-687.
[50] P. Alam, S. Dash, C. Climent, G. Kaur, A. R. Choudhury, D. Casanova, P. Alemany, R. Chowdhury, I. R. Laskar, *RSC Adv.* **2017**, *7*, 5642-5648.
[51] D. A. Ferrick, A. Neilson, C. Beeson, *Drug Discov. Today* **2008**, *13*, 268-274.
[52] W. H. Koppenol, P. L. Bounds, C. V. Dang, *Nat. Rev. Cancer* **2011**, *11*, 618-618.
[53] G. Kroemer, L. Galluzzi, P. Vandenabeele, J. Abrams, E. S. Alnemri, E. H. Baehrecke, M. V. Blagosklonny, W. S. El-Deiry, P. Golstein, D. R. Green, M. Hengartner, R. A. Knight, S. Kumar, S. A. Lipton, W. Malorni, G. Nunez, M. E. Peter, J. Tschopp, J. Yuan, M. Piacentini, B. Zhivotovsky, G. Melino, *Cell Death Differ.* **2009**, *16*, 3-11.
[54] S. Sperandio, K. Poksay, I. de Belle, M. J. Lafuente, B. Liu, J. Nasir, D. E. Bredesen, *Cell Death Differ.* **2004**, *11*, 1066-1075.
[55] R. C. Taylor, S. P. Cullen, S. J. Martin, *Nat. Rev. Mol. Cell Bio.* **2008**, *9*, 231-241.
[56] B. H. Li, J. O. Zhao, C. Z. Wang, J. Searle, T. C. He, C. S. Yuan, W. Du, *Cancer Lett.* **2011**, *301*, 185-192.
[57] K. M. Knopf, B. L. Murphy, S. N. MacMillan, J. M. Baskin, M. P. Barr, E. Boros, J. J. Wilson, *J. Am. Chem. Soc.* **2017**, *139*, 14302-14314.
[58] D. Hanahan, R. A. Weinberg, *Cell* **2011**, *144*, 646-674.
[59] X.-Y. Dai, J. Yan, X. Fu, Q. Pan, D. Sun, Y. Xu, J. Wang, L. Nie, L.-J. Tong, A. Shen, M. Zheng, M. Huang, M. Tan, H. Liu, X. Huang, J. Ding, M. Geng, *Clin. Cancer Res.* **2017**, *23*, 6267-6278.
[60] G. Will, G. Boschloo, S. N. Rao, D. Fitzmaurice, *J. Phys. Chem. B* **1999**, *103*, 8067-8079.
[61] F. X. Wang, M. H. Chen, X. Y. Hu, R. R. Ye, C. P. Tan, L. N. Ji, Z. W. Mao, *Sci. Rep.* **2016**, *6*, 38954.
[62] H. R. Wang, H. J. Zhong, R. Hou, J. Ayala, G. M. Liu, S. B. Yuan, Z. Yan, W. P. Zhang, Y. L. Liu, K. L. Cai, Z. G. Cai, H. Huang, Z. H. Zhang, D. Wu, *Sci. Rep.* **2017**, *7*, 3337.

10.1002/chem.201900851

WILEY-VCH

Entry for the Table of Contents
FULL PAPER

We report here two iridium complexes modified with anti-inflammatory drugs show multiple anticancer effects by disrupting the metabolism of cancer cells and regulating their immune functions. The aggregation of complexes in mitochondria can also be observed by phosphorescence lifetime imaging.

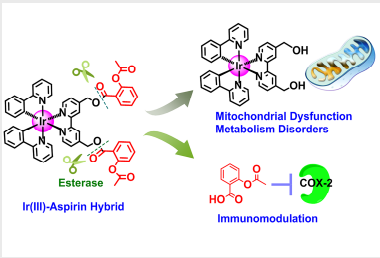

Xiao-Wen Wu, Yue Zheng, Fang-Xin Wang, Jian-Jun Cao, Hang Zhang, Dong-Yang Zhang, Cai-Ping Tan, Liang-Nian Ji, and Zong-Wan Mao**

Page No. – Page No.

Anticancer Ir(III)-Aspirin Conjugates for Enhanced Metabolic Immuno-Modulation and Mitochondrial Lifetime Imaging